# Harnessing nonlinear dynamics for quantum state synthesis of mechanical oscillators in tripartite optomechanics

Ryan O. Behunin
*Department of Applied Physics and Materials Science, Northern Arizona University, Flagstaff, Arizona 86011, USA*
*and Center for Materials Interfaces in Research and Applications (¡MIRA!), Northern Arizona University, Flagstaff, Arizona 86011, USA*

Peter T. Rakich
*Department of Applied Physics, Yale University, New Haven, Connecticut 06520, USA*

(Received 26 October 2022; revised 12 January 2023; accepted 31 January 2023; published 15 February 2023)

Owing to their long lifetimes at cryogenic temperatures, mechanical oscillators have been recognized as an attractive resource for quantum information science and as a test bed to explore fundamental physics. Key to many of these applications is the ability to prepare, manipulate, and measure quantum states of mechanical motion. By capturing the exact nonlinear quantum dynamics, we show how tripartite optomechanical interactions, involving the mutual coupling between two distinct optical modes and an acoustic resonance, enable quantum states of mechanical oscillators to be synthesized and interrogated using classical state preparation.

DOI: 10.1103/PhysRevA.107.023511

## I. INTRODUCTION

New methods to prepare and interrogate nonclassical states of mechanical oscillators could enable novel quantum technologies as well as the exploration of fundamental physics [1–12]. If the astounding lifetimes exhibited by phonons at cryogenic temperatures [2,13] can be translated to quantum coherence times, phononic systems could form the basis for high-dimensional quantum memories [14]. In addition, the ability to interrogate and manipulate these acoustic modes using superconducting qubits [15–18], electrical signals [2–4], or telecommunications wavelengths of light [7,8,13] makes them compelling candidates for quantum repeaters [14] and high-fidelity quantum state transfer [11,17,19], whereas mechanical oscillators with large effective mass may shed light on the quantum-to-classical transition [20,21], the nature of dark matter [12,22], and the impact of gravity on decoherence [1,23,24].

Generation, control, and measurement of quantum states of mechanical oscillators has recently been explored in a variety of electromechanical and optomechanical systems [15–17,25–31]. Within circuit systems, nonlinearity provided by a superconducting qubit has enabled quantum state preparation and readout in the mechanical domain [15–17,25,27,30,31]. Canonical cavity optomechanical interactions, which utilize nonlinear coupling between a single electromagnetic mode and a single mechanical mode (i.e., bipartite system), permit an array of state preparation, control, and readout functionalities [26,29,32–34]. By detuning a strong coherent drive from resonance, a linearized optomechanical coupling can be realized, enabling coherent state swaps between the mechanical and optical domains, ground-state cooling, entanglement generation, two-mode squeezing, and when combined with photon number measurements, the synthesis of single-phonon Fock states [26,29,32].

Looking beyond these demonstrations, it is challenging to access more exotic quantum states using conventional bipartite cavity optomechanical systems. While it is possible to create multicomponent cat states, macroscopically distinguishable superpositions, and phonon-photon entanglement if one can reach the ultrastrong coupling regime, this regime requires coupling rates on par with the phonon frequency [34]. Moreover, relatively weak optomechanical nonlinearities make this regime difficult to access with GHz-frequency phonons, which offer long coherence times at cryogenic temperatures. Alternatively, high-frequency phonons can be accessed using a tripartite system consisting of a single phonon mode that mediates coupling between two optical modes [7,8]. Moreover, the distinct structure of the tripartite system offers unique advantages as we consider new strategies to generate and detect exotic quantum states with mechanical systems, including robust entanglement generation, deterministic state preparation, and single-photon nonlinearities [35–41].

Here, we show that the nonlinear quantum dynamics of tripartite optomechanical systems can enable the preparation of highly nonclassical phononic states. Considering a triply resonant system, we explore the nonlinear dynamics of this tripartite system using the exact time evolution of the total system wave function, enabling analytical and numerical calculations for the quantum state dynamics [42–45]. Prior work has explored how tripartite coupling permits a variety of quantum features including sub-Poissonian field statistics, anticorrelations, and squeezing [42,43,46]. Our results show that experimentally accessible initial states (e.g., prepared using a coherent classical drive) evolve into wave functions exhibiting entanglement between optical and mechanical degrees of freedom. Leveraging this entanglement, we show that conditional measurements on the optical modes of the system, such

 

as homodyne detection and/or photon counting, can project the mechanical oscillator into highly nonclassical states that depend sensitively on the initial system wave function. By simulating the system evolution including the effects of decoherence, we identify regimes where quantum states can be robustly synthesized. Moreover, in the presence of a classical coherent drive, we show that the phonon's reduced density matrix exhibits nonclassicality even without state-collapsing conditional measurements. We also illustrate how $\pi/2$ and $\pi$ pulses can be used to entangle optical and mechanical modes, or transfer quantum states between the optical and mechanical domains.

While closely related, this tripartite system has important features not present in the canonical cavity optomechanical interaction that afford unique quantum dynamics. First, access to two optical modes greatly expands the number and complexity of the phonon states that can be heralded, where projective measurements produce families of phonon states parametrized by two sets of observables. Second, photon number measurements can herald highly nonclassical phonon states, in contrast with standard resonant cavity optomechanical interactions, even in systems with weak coupling [34]. Third, for telecommunications wavelengths of light the relevant phonon frequencies are of the order of $\sim$10 GHz, enabling ground state cooling with standard cryogenics. Put together, these results reveal an unexplored regime of nonlinear quantum dynamics in systems spanning from chip-scale optomechanical devices [9,10] to bulk crystals [7,8].

## II. QUANTUM DYNAMICS

To illustrate how quantum state generation can be accomplished using multimode optomechanical coupling, we explore the dynamics of a system described by the Hamiltonian $H = H_0 + H_{\text{int}}$,

$$H_0 = \hbar\omega_p a_p^\dagger a_p + \hbar\omega_S a_S^\dagger a_S + \hbar\Omega b^\dagger b,$$
$$H_{\text{int}} = \hbar g(a_p a_S^\dagger b^\dagger + a_p^\dagger a_S b). \tag{1}$$

Here, $a_p$, $a_S$, and $b$ are the annihilation operators of the pump, Stokes, and phonon modes, with angular frequencies $\omega_p$, $\omega_S$, and $\Omega$, respectively. This interaction Hamiltonian, $H_{\text{int}}$, describes phonon-mediated coupling between these two electromagnetic modes. Throughout, we assume that our system satisfies the condition $\omega_p = \omega_S + \Omega$, necessary for the phonon mode to mediate resonant coupling between the photon modes (i.e., intermodal scattering). Systems that are well described by this Hamiltonian typically utilize a high-frequency elastic wave to mediate resonant intermodal scattering (e.g., through Brillouin interactions [47]), with couplings ($g$) that can be produced by electrostriction or radiation pressure [48,49]. In the analysis that follows, we consider the dynamics of this system for times that are much shorter than the decoherence time of our phonon mode [15,31], permitting us to neglect the effects of phonon decoherence.

Neglecting decoherence, application of the time evolution operator to the initial wave function gives the quantum dynamics of this system in terms of the time-dependent wave function, given by the formal solution to the Schrödinger equation $|\psi(t)\rangle = \exp\{-iH_0 t/\hbar\}\exp\{-iH_{\text{int}}t/\hbar\}|\psi(0)\rangle$. Because $\omega_p = \omega_S + \Omega$, $H_0$ and $H_{\text{int}}$ commute, permitting the time-evolution operator to be factorized. While the operator $\exp\{-iH_{\text{int}}t/\hbar\}$ is an exponent of noncommuting operators, a symmetry of the system provides a path to a formal analytical solution: For a Fock state, the total number of phonons and pump photons $n_p + n_b$ (as well as $n_p + n_S$) is conserved, reducing the Hilbert space to a compact $(n_p + n_b + 1)$-dimensional subspace [42,43]. Within this compact Hilbert space, $H_{\text{int}}$ can be diagonalized, where the Hamiltonian given by Eq. (1) is formally equivalent to a Jaynes-Cummings model describing the interaction between a bosonic mode and a spin-$(n_p + n_b)/2$ system (see Ref. [42,43] and Appendix A) [50].

For the initial state $|n, m, 0\rangle \equiv |n\rangle_p \otimes |m\rangle_S \otimes |0\rangle_{ph}$, where the pump, Stokes, and phonon modes, respectively, have $n$, $m$, and 0 quanta and using Eq. (1), the time-dependent wave function $|\psi_{nm0}(t)\rangle$ in the interaction picture is generally represented by

$$|\psi_{nm0}(t)\rangle = \sum_{k=0}^{n} A_{n,m,k}(t)|n-k, m+k, k\rangle. \tag{2}$$

Truncation of the sum over $k$ at $n$ is a consequence of the compact nature of the Hilbert space for Fock state evolution [42]. Inserting $|\psi_{nm0}(t)\rangle$ into the Schrödinger equation yields a linear matrix differential equation for the complex probability amplitudes $A_{n,m,k}(t)$ given by

$$\dot{\vec{A}}_{n,m} = -i\mathbf{M}_{nm}\cdot\vec{A}_{n,m}. \tag{3}$$

Here, $\vec{A}_{n,m}$ is a column vector of the probability amplitudes $\vec{A}_{n,m} = (A_{n,m,n}, A_{n,m,n-1}, \ldots, A_{n,m,0})^T$, and $\mathbf{M}_{nm}$ is the symmetric matrix

$$\mathbf{M}_{nm} = \begin{pmatrix} 0 & \Lambda_n^{nm} & 0 & 0 & \cdots \\ \Lambda_n^{nm} & 0 & \Lambda_{n-1}^{nm} & 0 & \\ 0 & \Lambda_{n-1}^{nm} & 0 & 0 & \\ 0 & 0 & \ddots & & \vdots \\ \vdots & & & 0 & \Lambda_1^{nm} \\ & & \cdots & \Lambda_1^{nm} & 0 \end{pmatrix}, \tag{4}$$

with matrix elements given by $\Lambda_k^{nm} = g\sqrt{n-k+1}\sqrt{m+k}\sqrt{k}$. The solution to Eq. (3) can be obtained by diagonalizing the matrix $\mathbf{M}_{nm}$, yielding

$$\vec{A}_{n,m}(t) = \mathbf{V}_{nm}\cdot e^{-i\mathbf{\Omega}_{nm}t}\cdot\mathbf{V}_{nm}^\dagger\cdot\vec{A}_{n,m}(0), \tag{5}$$

where $\mathbf{V}_{nm}$ is a unitary matrix diagonalizing $\mathbf{M}_{nm}$, and the diagonal matrix of eigenvalues $\mathbf{\Omega}_{nm} = \mathbf{V}_{nm}^\dagger\cdot\mathbf{M}_{nm}\cdot\mathbf{V}_{nm}$ [51] (see Appendix B).

Focusing on initial states that can be prepared in the laboratory using classical light sources, photon squeezing, or single photon emitters, we calculate the system wave function. With the phonon cooled to the ground state, we consider initial wave functions given by

$$|\psi(0)\rangle = \sum_{n=0}^{\infty}\sum_{m=0}^{\infty}\mathcal{P}_n\mathcal{S}_m|n, m, 0\rangle, \tag{6}$$

where $\mathcal{P}_n$ ($\mathcal{S}_m$) is the probability amplitude for the pump (Stokes) mode to be found initially in the $n$th ($m$th) Fock state.

Using Eqs. (5) and (6), the time-dependent wave function is given by

$$|\psi(t)\rangle = \sum_{n,m=0}^{\infty}\sum_{k=0}^{n}\mathcal{P}_n\mathcal{S}_m A_{n,m,k}(t)|n-k, m+k, k\rangle, \quad (7)$$

with time-dependent coefficients $A_{n,m,k}(t)$ given by

$$A_{n,m,k}(t) = \hat{k}\cdot\mathbf{V}_{nm}\cdot e^{-i\mathbf{\Omega}_{nm}t}\cdot\mathbf{V}^{\dagger}_{nm}\cdot\vec{A}_{n,m}(0), \quad (8)$$

where $A_{n,m,k}(0) = \delta_{k0}$ and $\hat{k}$ is a unit vector of dimension $n+1$ given by $\hat{k} = (\delta_{n,k}, \delta_{n-1,k}, \ldots, \delta_{k0})$ [see Appendix C for a list of $A_{n,m,k}(t)$ for $n = 0$ to 2]. For optical states prepared with lasers $\mathcal{P}_n = \alpha_p^n \exp\{-|\alpha_p|^2/2\}/\sqrt{n!}$, describing a coherent state of amplitude $\alpha_p$, or for single photon emitters with $\mathcal{P}_n = \delta_{n1}$—definitions that also apply to the Stokes probability amplitudes $\mathcal{S}_m$. For example, when the system is prepared with a single pump photon, the wave function is given by [46]

$$|\psi(t)\rangle = \sum_{m=0}^{\infty}\mathcal{S}_m[\cos(g\sqrt{m+1}t)|1, m, 0\rangle - i\sin(g\sqrt{m+1}t)|0, m+1, 1\rangle]. \quad (9)$$

In this case, the total system dynamics is analogous to the Jaynes-Cummings model, exhibiting Rabi oscillations and coherent energy exchange between the three modes [42,43,50,52] (see Appendix A).

Even when the input optical fields are classical, quantum states can be generated. To illustrate, consider weak coherent states in the pump and Stokes modes, i.e., $|\alpha_p|, |\alpha_S| \ll 1$, where the initial photonic states are well approximated by a superposition of the vacuum and first excited states ($|\alpha_p\rangle \approx |0\rangle + \alpha_p|1\rangle$). In this limit the wave function is given by

$$|\psi(t)\rangle \approx |0,0,0\rangle + \alpha_S e^{-i\omega_S t}|0,1,0\rangle + + \alpha_p e^{-i\omega_p t}[\cos(gt)|1,0,0\rangle - i\sin(gt)|0,1,1\rangle] \quad (10)$$

to first order in $\alpha_p$ and $\alpha_S$, exhibiting quantum entanglement. For larger amplitudes, one must include more terms in the series representation of the wave function given in Eq. (7). However, for a classical initial state Fig. 1 shows a degradation of phonon-photon entanglement as the coherent state amplitude becomes large, consistent with the dynamics of this tripartite system in the limit that the pump and Stokes mode amplitudes can be treated as undepleted constants. Nevertheless, this example clearly illustrates how classical coherent states can be used to generate quantum states with resonant three-mode coupling (or with resonant coupling in this tripartite system).

These results show that resonant intermodal coupling coupling can produce entanglement between the mechanical oscillator and the optical modes, even for classically prepared initial states [e.g., Eq. (10)]. Looking beyond this analytical example of Eq. (10), we can use the linear entropy $S_L(t) \equiv 1 - \mathrm{Tr}\{\hat{\rho}_{ph}^2(t)\}$, where $\hat{\rho}_{ph}(t) = \mathrm{Tr}_{p,S}\{|\psi(t)\rangle\langle\psi(t)|\}$ is the reduced density matrix for the phonon mode, to analyze the degree of entanglement produced by more complex quantum states, evaluated through the numerical evaluation of Eq. (7). Figure 1 quantifies the entanglement between the phonon mode and the optical fields for a selection of initial states, exhibiting temporal oscillations determined by the coupling rate $g$, the initial state, and the eigenvalues $\mathbf{\Omega}_{nm}$. Using Eq. (7) summed to >99% convergence, Fig. 1 shows that phonon-photon entanglement persists for larger coherent state amplitudes.

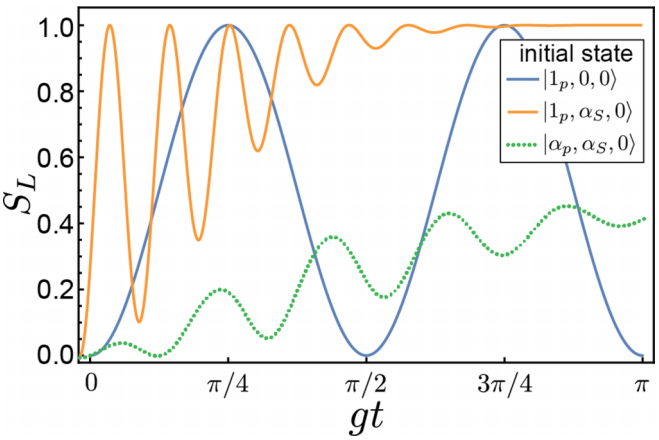


FIG. 1. Phonon linear entropy for experimentally accessible initial states. Coherent state amplitudes $\alpha_p = 1.0$ and $\alpha_S = 4.6$. For the single-pump photon initial states, the linear entropy is scaled by a factor 2 so that $S_L$ varies between 0 and 1. $S_L = 1$ indicates maximal phonon-photon entanglement.

## III. PREPARING AND MEASURING QUANTUM STATES OF A MECHANICAL MODE

Leveraging phonon-photon entanglement shown by Eq. (7) and Fig. 1, the phonon mode can be projected into a large variety of highly nonclassical states through conditional measurements of the optical fields. By applying the projective operator $\hat{P} = |\varphi_p, \varphi_S\rangle\langle\varphi_p, \varphi_S|$ to $|\psi(t)\rangle$, we obtain the phonon wave function $|\psi_{ph}[\varphi_p, \varphi_S, t)\rangle \equiv \langle\varphi_p, \varphi_S|\psi(t)\rangle$ resulting from the conditional measurement of the optical fields, with measurement outcomes given by $\varphi_p$ and $\varphi_S$ for the pump and Stokes modes, respectively. For example, for homodyne detection $\varphi_p$ represents the measured complex coherent state amplitude of the pump mode, or a photon number resolving measurement $\varphi_p$ indicates the measured number of pump photons.

Using homodyne detection, a projective measurement of the amplitude and phase of the optical modes in the interaction picture collapses the phonon wave function into the superposition of Fock states given by $|\psi_{ph}[\bar{\alpha}_p, \bar{\alpha}_S, t)\rangle = \sum_{k=0}^{\infty} c_k(t)|k\rangle$. Here, the unnormalized probability amplitudes $c_k(t)$ are given by

$$c_k(t) = \sum_{n=k}^{\infty}\sum_{m=0}^{\infty}\frac{\alpha_p^n(\bar{\alpha}_p^*)^{n-k}\alpha_S^m(\bar{\alpha}_S^*)^{m+k}}{\sqrt{n!}\sqrt{(n-k)!}\sqrt{m!}\sqrt{(m+k)!}} \times e^{-\frac{1}{2}(|\alpha_p|^2+|\bar{\alpha}_p|^2+|\alpha_S|^2+|\bar{\alpha}_S|^2)}A_{n,m,k}(t), \quad (11)$$

and $\bar{\alpha}_p$ and $\bar{\alpha}_S$ are the measured complex amplitudes for the pump and Stokes modes. For a given experimental configuration (i.e., input laser amplitudes and measured final

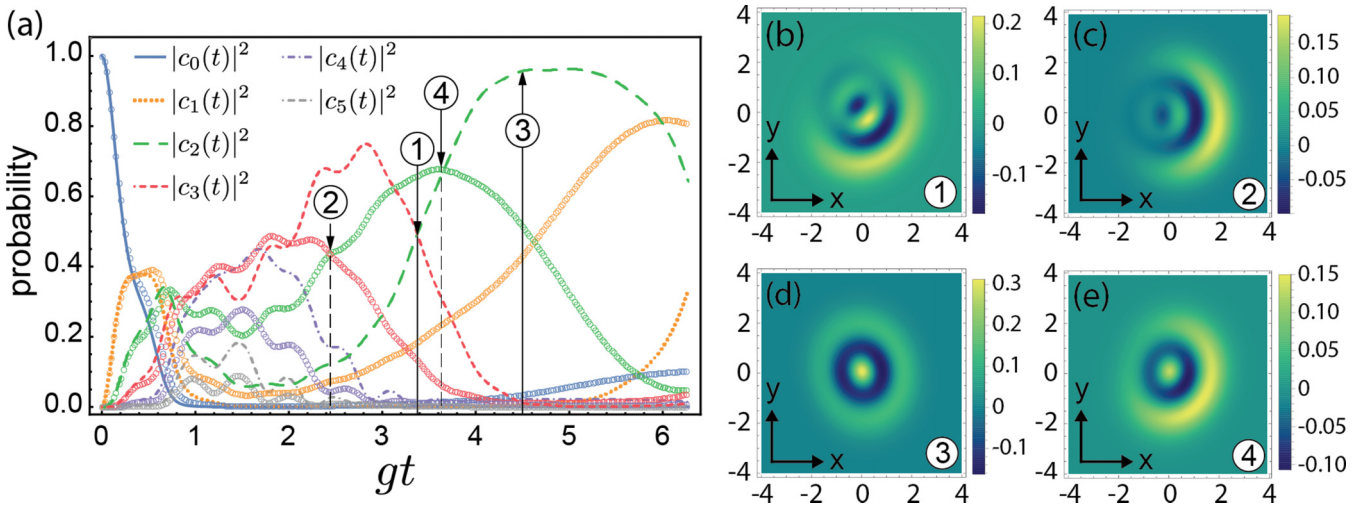


FIG. 2. Conditional quantum state preparation through homodyne measurements of the optical field. The initial state is $|\alpha_p, \alpha_S, 0\rangle$ and the optical fields are measured in state $|\bar{\alpha}_p, \bar{\alpha}_S\rangle$ at a later time. For $\alpha_p = 0.74$, $\alpha_S = 5.6$, $\bar{\alpha}_p = 0.01$, $\bar{\alpha}_S = 5.65\exp\{i0.3\pi\}$. (a) Phonon Fock state probabilities calculated from Eq. (11) (solid and dashed lines) and using a numerical master equation solver with damping for both pump and Stokes modes of $\gamma = 0.25g$ (open circles). (b–e) Wigner functions for targeted phonon states with and without optical losses. States approximating $|\psi_{ph}\rangle \approx (|2\rangle + |3\rangle\exp\{i\phi\})/\sqrt{2}$ shown in (b) $gt = 3.37$, denoted by ① (lossless) and (c) $gt = 2.63$, denoted by ② (optical losses). States approximating $|\psi_{ph}\rangle \approx |2\rangle$ shown in (d) $gt = 4.5$, denoted by ③ (lossless), and (e) $gt = 3.63$, denoted by ④ (optical losses). Fidelities for state preparation with losses are 72% for (c) and 67% for (e). The solid vertical lines correspond with the times where the Wigner function is computed for lossless dynamics, and dashed vertical lines correspond with times where the Wigner function is computed for the system with optical losses.

states), examination of the phonon Fock state probabilities as a function of time identify how certain states can be prepared [e.g., see Fig. 2(a)]. Such conditional measurements can collapse the phonon into a highly nonclassical state as shown in Figs. 2(b)–2(e). For example, in Fig. 2(b) the system occupies a nearly perfect superposition $|\psi_{ph}\rangle \approx (|2\rangle + |3\rangle\exp\{i\phi\})/\sqrt{2}$. Accounting for decoherence caused by optical losses, a master equation simulation [53] shows that this state can be achieved with 72% fidelity when the optical decay rates $\gamma = 0.25g$ (see Appendix E). With the large optomechanical coupling rates achievable in optomechanical crystals [54] (∼9 MHz), it is conceivable that future devices reach regimes where $\gamma \ll g$. However, even with larger optical losses, interesting states can still be accessed. By adjusting the initial optical state, entanglement generation can be accelerated so that targeted quantum states can be prepared at times $t < 1/\gamma$ (example below). Beyond this example, a tremendous range of nonclassical states become accessible by varying the amplitude and phases of initial and final photonic states as well as the measurement time.

It is important to note that the complex dynamics shown in Fig. 2 are a direct consequence of the nonlinearity intrinsic to Eqs. (1) and (7). For example, in the $\alpha_S \gg 1$ limit where $\alpha_S$ can be treated as a constant, the phonon excited state probabilities would exhibit periodic Rabi-like oscillations where the phonon state is given by a classical coherent state at each time (see Sec. IV).

We can also use Eq. (7) to identify opportunities for quantum state synthesis using conditional photon number resolving measurements. For example, when $|\psi(0)\rangle = |\alpha_p, \alpha_S, 0\rangle$ and when a single photon is measured in the pump and Stokes modes at time $t$, the phonon wave function collapses into the superposition of ground and excited states, expressed in unnormalized form as

$$|\psi_{ph}[1_p, 1_s, t)\rangle = \mathcal{N}\left[\alpha_S \cos(\sqrt{2}gt)|0\rangle - \frac{i\alpha_p}{\sqrt{6}}\sin(\sqrt{6}gt)|1\rangle\right], \tag{12}$$

where $\mathcal{N} = \alpha_p\mathcal{P}_0\mathcal{S}_0$. Although nondeterministic, manipulation of the initial state affords some control over the phonon wave function, e.g., by setting the amplitude $\alpha_S$ to zero the mechanical mode is guaranteed to be in a single phonon state.

Using single photon detection, we can illustrate how quantum state synthesis can be achieved with optical losses. Figure 3 shows the phonon Fock state probabilities, computed using Eq. (7) (solid lines) and a master equation solver (open circles), along with the phonon Wigner functions for the simulation with optical losses at selected times when a single Stokes photon is measured and the pump is measured using homodyne detection. This figure shows that even with optical decay rates of $50g$, a coherent superposition between ground and excited states and a single phonon state can be prepared with respective fidelities of 97% and 92%.

Even in the absence of conditional measurements, the mechanical oscillator can evolve into nonclassical states, leading to a form of deterministic state synthesis. In this case, the phonon mode is described by a reduced density matrix $\hat{\rho}_{\rm red}(t) = \sum_{k,k'=0}^{\infty}\rho_{kk'}(t)|k\rangle\langle k'|$ with matrix element given by

$$\rho_{kk'}(t) = \sum_{n=0}^{\infty}\sum_{m=\kappa}^{\infty}\mathcal{P}_{n+k}\mathcal{P}^*_{n+k'}\mathcal{S}_{m-k}\mathcal{S}^*_{m-k'} \times A_{n+k,m-k,k}(t)A^*_{n+k',m-k',k'}(t), \tag{13}$$

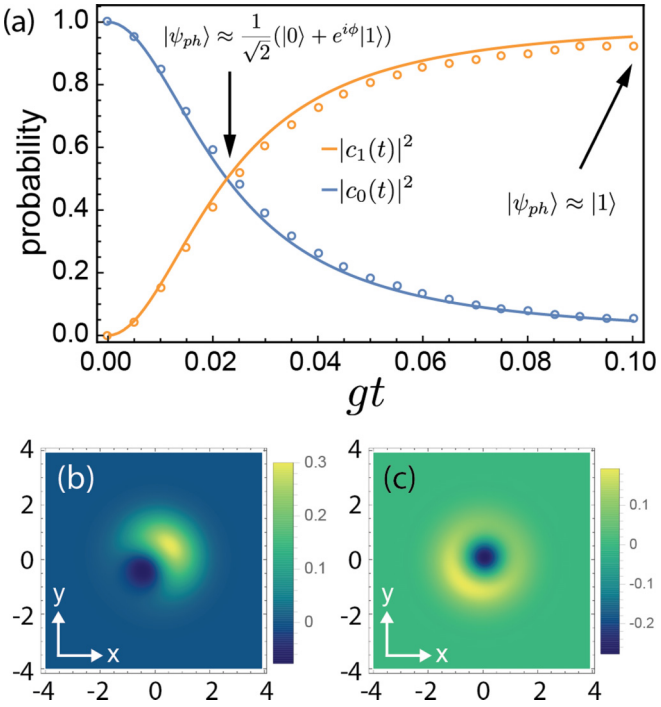


FIG. 3. Conditional quantum state preparation through single photon measurement of the Stokes mode and homodyne measurements of the pump. (a) Phonon Fock state probabilities capture the phonon wave function up to a phase, showing evolution into superposition and single phonon states. Fock state probabilities computed using Eq. (7) (lines) and a master equation solver including optical losses of decay rate $\gamma = 50g$ (open circles). (b and c) Plotted Wigner functions include the effects of optical losses, showing access to quantum states in the presence of optical losses. The initial state is $|\alpha_p, \alpha_S, 0\rangle$ with $\alpha_p = 4.41$ and $\alpha_S = 0.1$, and the measured complex amplitude of the pump is $\tilde{\alpha}_p = 3.7$.

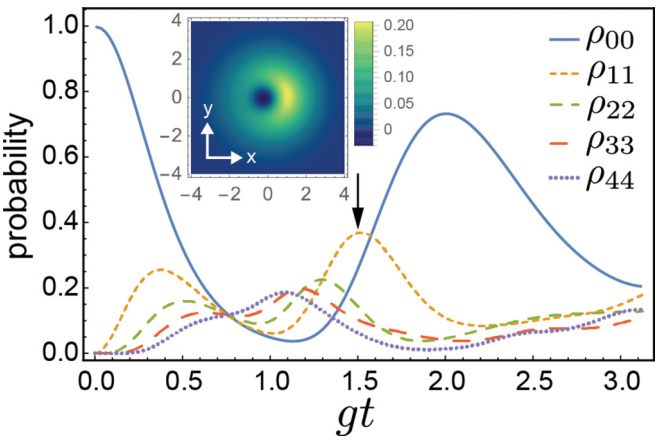


FIG. 4. Quantum states preparation in the absence of conditional optical measurements, i.e., when optical fields are traced out. The dynamics of the phonon occupation number probabilities (denoted by $\rho_{nn}$ for the $n$th Fock state) show times where the phonon wave function deviates from a classical state (e.g., $gt = 1.5$ where the Fock state probabilities do not follow the Poisson distribution). The initial state is $|\alpha_p, \alpha_S, 0\rangle$, with $\alpha_p = 2.4$ and $\alpha_S = 0.25$. Inset: Phonon Wigner function at $gt = 1.5$, showing a sharp deviation from a coherent state.

where $\kappa = \max(k, k')$. For a specific initial state, Fig. 4(a) illustrates how the Fock state probabilities for the phonon evolve in time, showing how a variety of nonclassical states can be prepared (Fig. 4). We emphasize that this behavior is a consequence of the quantum nonlinearity. Importantly, without the effects backreaction on the pump and the Stokes modes (e.g., pump depletion) provided by the nonlinear dynamics produced by Eq. (1), the phonon would evolve into a thermal or coherent state [55], and negativity of the Wigner function would not be possible.

## IV. QUANTUM STATE READOUT

In addition to providing a means to prepare quantum states of mechanical motion, $H_{\rm int}$ also enables state manipulation, transfer, and readout. When the Stokes mode is a large-amplitude coherent state (i.e., $|\alpha_S| \gg 1$), the $\exp\{-iH_{\rm int}t/\hbar\}$ is well approximated by the beam splitter transformation, transferring and entangling quantum states between the phononic and photonic domains [32]. Consider a phonon wave function given by a superposition of ground and excited states $|\psi_{ph}\rangle = c_0|0\rangle + c_1|1\rangle$. Equation (12) shows how this state can be prepared by conditional photon number resolving measurements. For the pump mode in the vacuum state and Stokes mode in a coherent state, the system wave function at time $t$ is

$$|\psi(t)\rangle = \sum_{m=0}^{\infty} \mathcal{S}_m[c_0|0, m, 0\rangle + c_1 \cos(\sqrt{m}gt)|0, m, 1\rangle - ic_1 \sin(\sqrt{m}gt)|1, m-1, 0\rangle]. \quad (14)$$

Under these assumptions, $\mathcal{S}_m$ is peaked at $m \sim |\alpha_S|^2$ with a standard deviation $\Delta m = |\alpha_S|$, allowing the arguments of the cosine and sine terms to be approximated by $\sqrt{m}gt \approx |\alpha_S|gt$ when $gt \ll 1$. Assuming the phase of $\alpha_S$ is $\pi/2$, these approximations give

$$|\psi(t)\rangle \approx c_0|0, \alpha_S, 0\rangle + c_1[\cos(|\alpha_S|gt)|0, \alpha_S, 1\rangle + \sin(|\alpha_S|gt)|1, \alpha_S, 0\rangle], \quad (15)$$

providing a "state swap" when $t = t_\pi \equiv \pi/(2|\alpha_S|g)$. For this generalized tripartite optomechanical $\pi$ pulse, $|\psi(t_\pi)\rangle \approx (c_0|0\rangle + c_1|1\rangle) \otimes |\alpha_S, 0\rangle$, showing how a quantum state in the mechanical domain can be transferred to the optical domain, where quantum state tomography can be performed. This result also shows how an optomechanical $\pi/2$ pulse ($|\alpha|gt_{\pi/2} = \pi/4$) can be used to prepare an entangled superposition of the pump and phonon. For $c_0 = 0$ and $c_1 = 1$, a phonon-photon Bell state is produced,

$$|\psi(t_{\pi/2})\rangle \approx \frac{1}{\sqrt{2}}[|0, \alpha_S, 1\rangle - ie^{i\varphi}|1, \alpha_S, 0\rangle], \quad (16)$$

where $\varphi$ is the phase of the Stokes mode. By sequencing these pulses, multimode optomechanical analogs of Ramsey interference and spin echo can be performed. While these results focus on the $|\alpha_S| \gg 1$ limit, Eq. (16) can be used to describe general state-swap dynamics.

## V. CONCLUSION

We have shown how the nonlinear dynamics produced by three-mode optomechanical coupling can be used to prepare and measure quantum states of a mechanical oscillator. Even with classically prepared initial states, these dynamics produce highly entangled photon-phonon states where conditional measurements on the optical fields can generate a wide variety of quantum states of the mechanical oscillator. Like conventional optomechanical interactions, this tripartite coupling permits the optomechanical equivalent of $\pi/2$ and $\pi$ pulses that can be used to entangle optical and mechanical states as well as transfer quantum information between the electromagnetic and mechanical domains. With long lifetimes at cryogenic temperatures, natural interface with telecommunications and radio frequency wavelengths, and large effective masses of phonon modes, our results may enable ways to manipulate quantum information stored in mechanical oscillators as well as tests of the foundations of quantum physics.

## ACKNOWLEDGMENTS

This work was supported by NSF Award No. 2145724 and ¡MIRA! ER Funds. The authors thank I. Montaño, D. Reiche, and S. Puri for stimulating discussions.

## APPENDIX A: FORMAL EQUIVALENCE BETWEEN THE MULTIMODE OPTOMECHANICAL HAMILTONIAN AND THE JAYNES-CUMMINGS MODEL

Leveraging the conservation of the number of pump photons and phonons and the Schwinger oscillator model of angular momentum [56], a formal analogy between the multimode optomechanical Hamiltonian and the Jaynes-Cummings (JC) model [50] can be derived. To reveal this relationship, we define the following pseudospin operators:

$$\hat{N} = (\hat{n}_p + \hat{n}_b)/2 \tag{A1}$$

$$S_z = (\hat{n}_p - \hat{n}_b)/2 \tag{A2}$$

$$S_- = a_p b^\dagger \tag{A3}$$

$$S_+ = a_p^\dagger b, \tag{A4}$$

where $\hat{n}_p$ and $\hat{n}_b$ are the number operators for the pump and phonon modes, respectively. The commutation relations of $a_p$ and $b$ show that the pseudospin operators obey the relations

$$[\hat{N}, S_z] = 0 \tag{A5}$$

$$[S_z, S_\pm] = \pm S_\pm \tag{A6}$$

$$[S_+, S_-] = 2S_z. \tag{A7}$$

Furthermore, one can show that $N$, the eigenvalue for $\hat{N}$, plays the role for the total spin, that these operators have all of the expected effects on Fock states $|n_p, n_b\rangle$ where the eigenvalues of $S_z$, $m \equiv (n_p - n_b)/2$, correspond with the azimuthal component of the pseudospin along the $z$ axis. For example, using $N$ and $m$, a generic Fock state $|n_p, n_b\rangle$ can be formally expressed as $|N, m\rangle$ ($n_p = N + m$ and $n_b = N - m$), where the operators above have acted in a manner analogous to a spin system:

$$S_z|N, m\rangle = m|N, m\rangle \tag{A8}$$

$$S_\pm|N, m\rangle = \sqrt{N \pm m + 1}\sqrt{N \mp m}|N, m \pm 1\rangle \tag{A9}$$

$$\mathbf{S}^2|N, m\rangle = (S_z^2 - S_z + S_+S_-)|N, m\rangle \tag{A10}$$

$$= N(N+1)|N, m, j\rangle. \tag{A11}$$

Using these operators and the phase-matching conditions, one can show that

$$H \to \hbar(\omega_p + \Omega)N + \hbar\omega_S S_z + \hbar\omega_S a_S^\dagger a_S + \hbar g(S_- a_S^\dagger + S_+ a_S), \tag{A12}$$

demonstrating the equivalence between the multimode Hamiltonian and the JC model when $N$ is fixed. In general, initial states that can be prepared in the laboratory will contain a superposition of different $N$ states, such as coherent states. Therefore, the multimode optomechanical dynamics of realistic systems is complex, involving several pseudospins, with distinct spin $N$, interacting with a bosonic mode.

## APPENDIX B: DIAGONALIZATION OF $\mathbf{M}_{nm}$

The formal solution to Eq. (3) can be obtained by diagonalizing $\mathbf{M}_{nm}$. By solving the eigenvalue equation $\mathbf{M}_{nm} \cdot \vec{E}_{nm,k} = \Omega_{nm,k}\vec{E}_{nm,k}$, where $\vec{E}^*_{nm,k} \cdot \vec{E}_{nm,k'} = \delta_{k,k'}$, the eigenvalues can be obtained as well as the unitary matrix $\mathbf{V}_{nm}$. Comprising a matrix of the normalized eigenvectors of $\mathbf{M}_{nm}$, the definition of $\mathbf{V}_{nm}$ is

$$\mathbf{V}_{nm} = (\vec{E}_{nm,n}, \quad \vec{E}_{nm,n-1}, \quad \ldots, \quad \vec{E}_{nm,0}). \tag{B1}$$

For example, for $n_p + n_b = 1$, the normalized eigenvectors are

$$\vec{E}_{1m,1} = \frac{1}{\sqrt{2}}\begin{pmatrix}1\\1\end{pmatrix}, \quad \vec{E}_{1m,0} = \frac{1}{\sqrt{2}}\begin{pmatrix}-1\\1\end{pmatrix}, \tag{B2}$$

giving $\mathbf{V}_{1m}$

$$\mathbf{V}_{1m} = \frac{1}{\sqrt{2}}\begin{pmatrix}1 & -1\\1 & 1\end{pmatrix}. \tag{B3}$$

Using $\mathbf{V}_{1m}$ to diagonalize $\mathbf{M}_{1m}$, we obtain the diagonal matrix of eigenvalues $\mathbf{\Omega}_{1m}$,

$$\mathbf{V}_{1m}^\dagger \cdot \mathbf{M}_{1m} \cdot \mathbf{V}_{1m} \equiv \mathbf{\Omega}_{1m} = g\sqrt{m+1}\begin{pmatrix}1 & 0\\0 & -1\end{pmatrix}. \tag{B4}$$

## APPENDIX C: PROBABILITY AMPLITUDE TIME DYNAMICS

Here we list the first few terms $A_{n,m,k}(t)$. By solving Eq. (3), assuming the phonon is initially in the ground state, we find

$$A_{0,m,0}(t) = 1 \tag{C1}$$

$$A_{1,m,0}(t) = \cos(\sqrt{m+1}gt) \tag{C2}$$

$$A_{1,m,1}(t) = -i\sin(\sqrt{m+1}gt)1 \tag{C3}$$

$$A_{2,m,0}(t) = \frac{2 + m + (1+m)\cos(\sqrt{4m+6}gt)}{3+2m} \tag{C4}$$

$$A_{2,m,1}(t) = -i\sqrt{\frac{1+m}{3+2m}}\sin(\sqrt{4m+6}gt) \quad \text{(C5)}$$

$$A_{2,m,2}(t) = -2\frac{\sqrt{(1+m)(2+m)}}{3+2m}\sin^2(\sqrt{m+3/2}gt). \quad \text{(C6)}$$

## APPENDIX D: GENERAL EXPRESSION FOR THE WIGNER FUNCTION

The phonon Wigner function is given by

$$W(\alpha) = \frac{1}{2\pi^2}\int d^2\xi\; e^{\alpha\xi^* - \alpha^*\xi}\mathrm{Tr}[\hat{\rho}D(\xi)], \quad \text{(D1)}$$

where $\alpha \equiv (x+iy)/\sqrt{2}$, $x$ and $y$ are dimensionless position and momentum quadratures, and $D(\xi)$ is the phonon displacement operator [55]. Here, $\hat{\rho}$ is either the reduced phonon density matrix or the density matrix obtained after conditional measurement of the optical fields.

For a general state expressed in the Fock basis (i.e., $\rho_{kk'}$), the Wigner function is given by

$$W(\alpha) = \frac{1}{\pi}\sum_{k,k'=0}^{\infty}\frac{(-1)^k 2^{k'-k}}{\sqrt{k!}\sqrt{k'!}}(\partial_\alpha - 2\alpha^*)^k \alpha^{k'} e^{-2\alpha\alpha^*}\rho_{kk'}, \quad \text{(D2)}$$

where $\rho_{kk'} = c_k c_{k'}^*$ for a pure state and $c_k$ is the phonon probability amplitude for the $k$th Fock state.

For the case where the optical fields are conditionally measured, the general expression for the phonon Wigner function can be computed by making the following replacement in Eq. (D1):

$$\mathrm{Tr}[\hat{\rho}D(\xi)] \to \langle\psi_{ph}[\varphi_p, \varphi_S, t)|D(\xi)|\psi_{ph}[\varphi_p, \varphi_S, t)\rangle. \quad \text{(D3)}$$

## APPENDIX E: EFFECTS OF OPTICAL LOSSES FROM MASTER EQUATION SIMULATIONS

For the assessment of decoherence caused by optical losses, we simulate the quantum dynamics of this tripartite optomechanical system [53]. We solve the Linblad form of the master equation, capturing the decay of both optical modes at a rate $\gamma$ given by

$$\dot{\rho} = -\frac{i}{\hbar}[H, \rho] + \frac{\gamma}{2}\sum_{j=p,S}[2a_j\rho a_j^\dagger - a_j^\dagger a_j\rho - \rho a_j^\dagger a_j]. \quad \text{(E1)}$$

Given the high frequency of the photon modes, Eq. (E1) assumes a bath temperature of zero.


[1] W. Marshall, C. Simon, R. Penrose, and D. Bouwmeester, Phys. Rev. Lett. **91**, 130401 (2003).

[2] M. Goryachev, D. L. Creedon, E. N. Ivanov, S. Galliou, R. Bourquin, and M. E. Tobar, Appl. Phys. Lett. **100**, 243504 (2012).

[3] M. Goryachev, D. L. Creedon, S. Galliou, and M. E. Tobar, Phys. Rev. Lett. **111**, 085502 (2013).

[4] S. Galliou, M. Goryachev, R. Bourquin, P. Abbé, J. P. Aubry, and M. E. Tobar, Sci. Rep. **3**, 2132 (2013).

[5] A. Lo, P. Haslinger, E. Mizrachi, L. Anderegg, H. Müller, M. Hohensee, M. Goryachev, and M. E. Tobar, Phys. Rev. X **6**, 011018 (2016).

[6] M. E. Tobar, New J. Phys. **19**, 091001 (2017).

[7] W. Renninger, P. Kharel, R. Behunin, and P. Rakich, Nat. Phys. **14**, 601 (2018).

[8] P. Kharel, Y. Chu, M. Power, W. H. Renninger, R. J. Schoelkopf, and P. T. Rakich, APL Photonics **3**, 066101 (2018).

[9] M. Eichenfield, R. Camacho, J. Chan, K. J. Vahala, and O. Painter, Nature (London) **459**, 550 (2009).

[10] M. Eichenfield, J. Chan, R. M. Camacho, K. J. Vahala, and O. Painter, Nature (London) **462**, 78 (2009).

[11] M. J. Weaver, F. Buters, F. Luna, H. Eerkens, K. Heeck, S. de Man, and D. Bouwmeester, Nat. Commun. **8**, 824 (2017).

[12] W. M. Campbell, B. T. McAllister, M. Goryachev, E. N. Ivanov, and M. E. Tobar, Phys. Rev. Lett. **126**, 071301 (2021).

[13] G. S. MacCabe, H. Ren, J. Luo, J. D. Cohen, H. Zhou, A. Sipahigil, M. Mirhosseini, and O. Painter, Science **370**, 840 (2020).

[14] M. Pechal, P. Arrangoiz-Arriola, and A. H. Safavi-Naeini, Quantum Sci. Technol. **4**, 015006 (2018).

[15] Y. Chu, P. Kharel, W. H. Renninger, L. D. Burkhart, L. Frunzio, P. T. Rakich, and R. J. Schoelkopf, Science **358**, 199 (2017).

[16] Y. Chu, P. Kharel, T. Yoon, L. Frunzio, P. T. Rakich, and R. J. Schoelkopf, Nature (London) **563**, 666 (2018).

[17] E. A. Wollack, A. Y. Cleland, R. G. Gruenke, Z. Wang, P. Arrangoiz-Arriola, and A. H. Safavi-Naeini, Nature (London) **604**, 463 (2022).

[18] R. Manenti, A. F. Kockum, A. Patterson, T. Behrle, J. Rahamim, G. Tancredi, F. Nori, and P. J. Leek, Nat. Commun. **8**, 975 (2017).

[19] A. Reed, K. Mayer, J. Teufel, L. Burkhart, W. Pfaff, M. Reagor, L. Sletten, X. Ma, R. Schoelkopf, E. Knill *et al.*, Nat. Phys. **13**, 1163 (2017).

[20] G. C. Ghirardi, P. Pearle, and A. Rimini, Phys. Rev. A **42**, 78 (1990).

[21] I. C. Percival, Proc. R. Soc. London, Ser. A **447**, 189 (1994).

[22] J. Manley, D. J. Wilson, R. Stump, D. Grin, and S. Singh, Phys. Rev. Lett. **124**, 151301 (2020).

[23] L. Diósi, Phys. Rev. A **40**, 1165 (1989).

[24] R. Penrose, Found. Phys. **44**, 557 (2014).

[25] A. D. O'Connell, M. Hofheinz, M. Ansmann, R. C. Bialczak, M. Lenander, E. Lucero, M. Neeley, D. Sank, H. Wang, M. Weides *et al.*, Nature (London) **464**, 697 (2010).

[26] T. Palomaki, J. Teufel, R. Simmonds, and K. W. Lehnert, Science **342**, 710 (2013).

[27] T. Aref, P. Delsing, M. K. Ekström, A. F. Kockum, M. V. Gustafsson, G. Johansson, P. J. Leek, E. Magnusson, and R. Manenti, *Superconducting Devices in Quantum Optics* (Springer, New York, 2016), pp. 217–244.

[28] W. H. P. Nielsen, Y. Tsaturyan, C. B. Møller, E. S. Polzik, and A. Schliesser, Proc. Natl. Acad. Sci. USA **114**, 62 (2017).

[29] S. Hong, R. Riedinger, I. Marinković, A. Wallucks, S. G. Hofer, R. A. Norte, M. Aspelmeyer, and S. Gröblacher, Science **358**, 203 (2017).

[30] L. R. Sletten, B. A. Moores, J. J. Viennot, and K. W. Lehnert, Phys. Rev. X **9**, 021056 (2019).

[31] K. J. Satzinger, Y. Zhong, H.-S. Chang, G. A. Peairs, A. Bienfait, M.-H. Chou, A. Cleland, C. R. Conner, É. Dumur, J. Grebel *et al.*, Nature (London) **563**, 661 (2018).

[32] M. Aspelmeyer, T. J. Kippenberg, and F. Marquardt, Rev. Mod. Phys. **86**, 1391 (2014).
[33] S. Mancini, V. I. Man'ko, and P. Tombesi, Phys. Rev. A **55**, 3042 (1997).
[34] S. Bose, K. Jacobs, and P. L. Knight, Phys. Rev. A **56**, 4175 (1997).
[35] P. Kómár, S. D. Bennett, K. Stannigel, S. J. M. Habraken, P. Rabl, P. Zoller, and M. D. Lukin, Phys. Rev. A **87**, 013839 (2013).
[36] Y.-D. Wang, S. Chesi, and A. A. Clerk, Phys. Rev. A **91**, 013807 (2015).
[37] N. Lörch and K. Hammerer, Phys. Rev. A **91**, 061803(R) (2015).
[38] J.-Q. Liao and L. Tian, Phys. Rev. Lett. **116**, 163602 (2016).
[39] X. Yang, Y. Ling, X. Shao, and M. Xiao, Phys. Rev. A **95**, 052303 (2017).
[40] M. Brunelli, O. Houhou, D. W. Moore, A. Nunnenkamp, M. Paternostro, and A. Ferraro, Phys. Rev. A **98**, 063801 (2018).
[41] D.-G. Lai, Y.-H. Chen, W. Qin, A. Miranowicz, and F. Nori, Phys. Rev. Res. **4**, 033112 (2022).
[42] D. F. Walls and R. Barakat, Phys. Rev. A **1**, 446 (1970).
[43] D. Walls and C. Tindle, J. Phys. A: Gen. Phys. **5**, 534 (1972).
[44] B. Jurčo, J. Math. Phys. **30**, 1739 (1989).
[45] S. Carusotto, Phys. Rev. A **40**, 1848 (1989).
[46] G. Drobný and I. Jex, Phys. Rev. A **46**, 499 (1992).
[47] P. Kharel, G. I. Harris, E. A. Kittlaus, W. H. Renninger, N. T. Otterstrom, J. G. Harris, and P. T. Rakich, Sci. Adv. **5**, eaav0582 (2019).
[48] P. T. Rakich, C. Reinke, R. Camacho, P. Davids, and Z. Wang, Phys. Rev. X **2**, 011008 (2012).
[49] P. Kharel, R. O. Behunin, W. H. Renninger, and P. T. Rakich, Phys. Rev. A **93**, 063806 (2016).
[50] E. T. Jaynes and F. W. Cummings, Proc. IEEE **51**, 89 (1963).
[51] G. B. Arfken and H. J. Weber, *Mathematical Methods for Physicists*, 6th ed. (Elsevier Academic Press, New York, 2005).
[52] B. W. Shore and P. L. Knight, J. Mod. Opt. **40**, 1195 (1993).
[53] J. R. Johansson, P. D. Nation, and F. Nori, Comput. Phys. Commun. **183**, 1760 (2012).
[54] J. Chan, M. Eichenfield, R. Camacho, and O. Painter, Opt. Express **17**, 3802 (2009).
[55] C. Gerry, P. Knight, and P. L. Knight, *Introductory Quantum Optics* (Cambridge University Press, Cambridge, 2005).
[56] J. Schwinger, On angular momentum, Report No. NYO-3071 (Nuclear Development Associates, 1952) (unpublished).